Size-Tuned Plastic Flow Localization in Irradiated Materials at the Submicron Scale

Yinan Cui,* Giacomo Po, and Nasr Ghoniem
Mechanical and Aerospace Engineering Department, University of California, 420 Westwood Plaza, Los Angeles, California 90095, USA

(Received 8 November 2017; published 22 May 2018)

Three-dimensional discrete dislocation dynamics (3D-DDD) simulations reveal that, with reduction of sample size in the submicron regime, the mechanism of plastic flow localization in irradiated materials transitions from irradiation-controlled to an intrinsic dislocation source controlled. Furthermore, the spatial correlation of plastic deformation decreases due to weaker dislocation interactions and less frequent cross slip as the system size decreases, thus manifesting itself in thinner dislocation channels. A simple model of discrete dislocation source activation coupled with cross slip channel widening is developed to reproduce and physically explain this transition. In order to quantify the phenomenon of plastic flow localization, we introduce a "deformation localization index," with implications to the design of radiation-resistant materials.

DOI: 10.1103/PhysRevLett.120.215501

Deformation localization is a manifestation of the complex physics controlling plastic instabilities, self-organization, and fracture initiation [1–4]. It is a significant concern in fundamental science and a wide variety of applications, including geophysical solid deformation [3], machinability [2], and the design of reliable materials [4–6]. In particular, deformation localization is widely observed in irradiated materials, where the phenomenon is manifested in the formation of defect-free dislocation channels, which can lead to the drastic deterioration of structural materials in nuclear energy [4,7–9]. Extensive experimental and modeling efforts have been carried out to shed light on the mechanisms that lead to irradiation-induced deformation localization [4,7–12]. It has been found that during plastic deformation, the movement of dislocations may sweep away, absorb, or destroy irradiation-produced defects. These nanoscale events are responsible for dislocation channel formation and deformation localization. However, and until now, a clear quantitative understanding of what determines the width of dislocation channels and the influence of sample size remain as challenging questions [13,14]. The main difficulty resides in the paucity of systematic experiments under controlled conditions and the significant computational difficulties because of the high density of nanoscale irradiation defects [12–14].

In this Letter, a new computer simulation method based on three-dimensional discrete dislocation dynamics (3D-DDD) combined with a field description of nanoscale defects is presented to circumvent these difficulties. The method affords a unique opportunity to study the physical mechanisms that influence size effects in a quantitative manner, and thus, it can close the gap between computational and experimental investigations. We present the first 3D-DDD observations on the size-tuned dislocation channel formation process to answer key questions. These are: (i) To what extent deformation is localized in irradiated materials? (ii) What determines the dislocation channel width? (iii) How does deformation localization depend on the external sample size? Such quantitative analysis on the extent of plastic slip localization is lacking, and this study unveils the answers to these critical questions. The results directly shed light on understanding experiments on small-scale mechanical testing of irradiated materials. This type of testing is gaining popularity due to the benefits of accelerated research, the reduction of radiation exposure, and the utilization of shallow ion-beam irradiation [9,13–16]. In addition, understanding the physics of channel formation holds the promise of developing new concepts for the design of advanced radiation-resistant polycrystalline and microarchitectured materials.

The 3D-DDD employed here are one part of the MoDELib (Mechanics Of Defect Evolution Library) software system [17], which is described in detail in our previous papers [18,19]. In this approach, curved dislocation lines are discretized into a succession of parametrized segments. A system of equations for the motion of nodes connecting these segments is solved in a way similar to the traditional finite element method (FEM). Boundary conditions and image forces are considered by coupling the infinite domain solution with an FEM-based boundary correction problem. Furthermore, we have demonstrated that the DDD method reproduces fundamental atomistic interaction mechanisms between dislocations and irradiation defects [20]. However, because of the high density of radiation-induced defects, massive simulations of discrete interactions between dislocations and all radiation defects are computationally prohibitive (e.g., Ref. [12]), thus limiting the simulation volume size and type of defects

involved. Until now, only a small number of 3D-DDD simulations on dislocation channel formation have been reported [4,10,12]. To overcome the computational difficulty, we developed a 3D-DDD method coupled with a *continuum* irradiation defect field. We first determine the dislocation resistance stress and destruction rate of irradiation defects using small volumes containing discrete defects and dislocations. Then, in massive simulations, the defect field is considered as continuous, where its density evolves according to a conservation equation. In turn, the continuum defect evolution equation is coupled with DDD through spatially-dependent annihilation rate and resistance stress. The method, which overcomes the difficulty of the excessive number of equations to be solved in discrete calculations (several hundred thousands), is detailed in our publications [20–22].

We performed an extensive series of 3D-DDD simulations of tension tests of Fe micropillars along the [001] direction at 320 K. The pillar size was varied in the range 300–1500 nm, and the irradiation defect density range was $10^{21} - 3 \times 10^{22}$ m^{-3} for comparison with experiments [35]. Figure 1 shows typical dislocation configurations and the irradiation defect distributions after deformation. Clear dislocation channels in Fe are observed only at a high irradiation dose (defect density), as shown in Figs. 1(a), 1(c), 1(e), and 1(g), in agreement with experiments [35]. The calculated channel width also agrees with experiments (50–200 nm [35,36] on bulk specimens), as indicated in Fig. 1, and it decreases with reducing the sample size. One notices that when the sample size is very small, the channel size is comparable with the irradiation-induced defect spacing, obviating the distinction of dislocation channels at submicron scales.

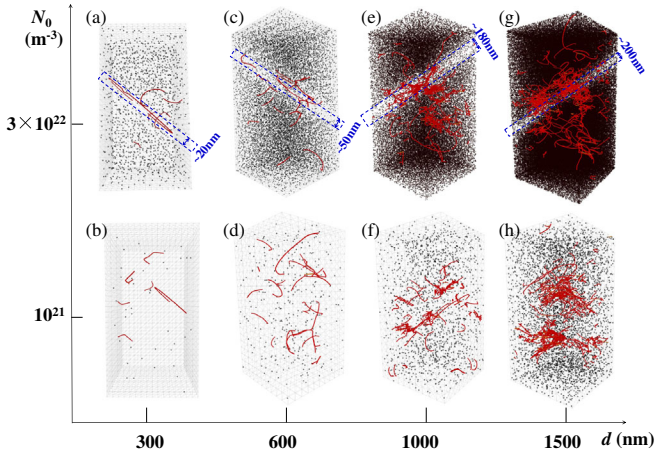

FIG. 1. Snapshots of irradiation defect (dark grey dots) and dislocation (red lines) distributions in irradiated Fe pillars with a diameter (a)–(b) $d = 300$ nm, (c)–(d) $d = 600$ nm, (e)–(f) $d = 1000$ nm, and (g)–(h) $d = 1500$ nm when the plastic strain is 6% for (a)–(b) and 2% for (c)–(h). Blue dotted regions denote dislocation channels.

To quantitatively discuss plastic flow localization, it is highly desirable to condense the complex 3D deformation information into some easy-to-handle parameters. We therefore proceed here to establish a generally-applicable deformation localization index (DLI). We define the DLI as the percent of the specimen volume whose plastic strain γ^p is lower than its volume-averaged value ($\bar{\gamma}^p$). For the extreme case of homogeneous deformation, there is no volume that has $\gamma^p < \bar{\gamma}^p$, and thus, the DLI = 0. On the other hand, if γ^p is highly localized in a very small region, then, the DLI is close to 1. Experimentally, the DLI can be estimated from statistical analysis of surface step distributions [22]. Figure 2(a) clearly demonstrates that, for large samples, increasing the irradiation dose significantly increases the DLI, in agreement with the expectation of irradiation-induced deformation localization. For bulk (or large samples), this can be understood as follows. In a bulk irradiated sample, the activation stress of a dislocation source τ_s is calculated as

$$\tau_s = \tau_0 + \alpha_1 \mu b \sqrt{\rho} + \alpha_2 \mu b \sqrt{Na}, \tag{1}$$

where the three terms on the right-hand side represent the lattice resistance stress, Taylor hardening induced by forest dislocations, and the resistance stress induced by irradiation defects, respectively. μ is the shear modulus, b is the magnitude of Burgers vector, α_1 is a dimensionless constant, and ρ is the dislocation density. α_2 represents an average value of the irradiation defect strength [21]. N and a represent the volume density and average size of irradiation defects, respectively. $(Na)^{-1/2}$ characterizes the average distance between irradiation defects on the slip plane. If some dislocation sources are activated, localized deformation will be observed if τ_s decreases during deformation. Namely, $d\tau_s/d\gamma^p < 0$. The evolution of ρ and N can be expressed as [21,37],

$$\frac{d\rho}{d\gamma^p} = \frac{1}{b l_{fr}} - \frac{y_a \rho}{b}, \qquad l_{fr} = \frac{1}{k_m \sqrt{\rho}} \tag{2}$$

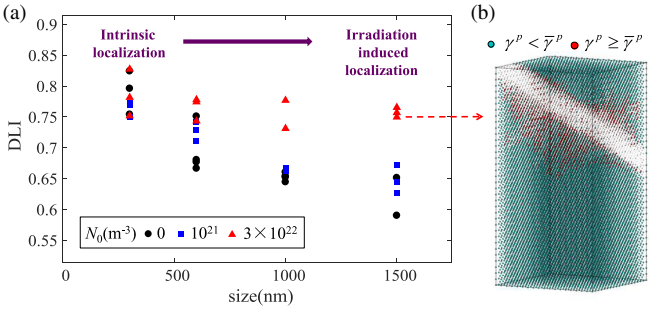

FIG. 2. (a) DLI for unirradiated and irradiated pillars when the plastic strain is 2.0%. (b) An example showing the correlation between a high DLI and dislocation channel formation, γ^p and $\bar{\gamma}^p$ is local and volume-averaged plastic shear strain, respectively. The symbol size is proportional to the local irradiation defect density

$$\frac{dN}{d\gamma^p} = -\lambda y \frac{N}{b}, \tag{3}$$

where l_{fr} is the dislocation mean free path, k_m is a dimensionless constant. y_a is the effective mutual annihilation distance between dislocations of opposite sign. In Eq. (3), y describes the capture distance, below which irradiation defect clusters might be absorbed or swept away by gliding dislocations, and λ is the irradiation defect annihilation fraction [21]. We obtain

$$\frac{d\tau_s}{d\gamma^p} = \frac{\alpha_1 \mu}{2}\left(k_m - y_a\sqrt{\rho} - \frac{\alpha_2}{\alpha_1}\lambda y\sqrt{Na}\right) < 0 \tag{4}$$

$$N > \frac{\alpha_1^2(k_m - y_a\sqrt{\rho})^2}{\alpha_2^2\lambda^2 y^2 a}. \tag{5}$$

Equation (4) clearly shows that plastic instability occurs when the dislocation multiplication effect [the first two terms on the rhs of Eq. (4)] is weaker than the irradiation defect clearing effect [the third term in Eq. (4)]. Equation (5) suggests that high dose irradiation is conducive to triggering plastic softening and the possibility of dislocation channel formation when the defect density is greater than the critical value given by Eq. (5). For example, in irradiated bulk Fe, dislocation channels are experimentally observed when $N = 5 \times 10^{21}$ m^{-3}, but not when $N = 1 \times 10^{21}$ m^{-3} [35]. This agrees well with the predictions of Eq. (5), from which we calculate the critical irradiation defect density as $N_c = 4.5 \times 10^{21}$ m^{-3}. The parameters are set according to experiments [35] ($\rho = 10^{12}$ m^{-2}, $a = 5$ nm) and Table I. Note that, the results presented here are representative of low strain rate loading (i.e., quasistatic), where high strain rate effects are ignored [8].

By contrast, Fig. 2(a) demonstrates that at small scales, the intrinsic deformation localization (induced by internal dislocation structure instead of irradiation defects) is already very pronounced, even for unirradiated materials. This agrees with experimental observation of highly localized deformation at the submicron scale [41]. Figure 1(a) illustrates that the dislocation source number in small pillars is very limited, which is significantly different from the highly tangled dislocation configurations observed in Figs. 1(e)–1(h) of larger size pillars. The deformation is prone to being concentrated around the position of activated dislocation sources. Weak dislocation interactions provide the possibility of continuous operation of available sources without tangling with other dislocations. It is the operation of the limited single-arm dislocation sources that leads to the highly localized deformation mode of unirradiated, submicron pillars.

Size-dependent localization also manifests itself through various spatial correlations. Figure 2(b) shows that in large samples, the high plastic strain zone ($\gamma^p > \bar{\gamma}^p$ according to the definition of DLI) is densely populated within a thick dislocation channel region. This illustrates the correspondence between a high value of the DLI parameter and the observation of dislocation channels in bulklike samples [22]. Conversely, the high plastic strain zone in small samples is sometimes distributed in several slip regions [such as Fig. 3(a)]. Heavily deformed zones are associated with much thinner dislocation channels. The width of the dislocation channel is clearly found to be controlled by the cross slip mechanism. In bulklike irradiated samples, the dislocation channel size is significantly reduced if the cross slip mechanism is deactivated [such as Figs. 3(c)–(d)]. This is consistent with the general belief that cross slip is an important mechanism leading to the widening of dislocation channels [4,11]. However, at small scales, cross slip plays a weak role in controlling the channel width [Figs. 3(a)–(b)]. This implies that the much thinner dislocation channels observed at small scales are associated with less frequent cross slip events as a result of the limited dislocation mean free path.

With the aid of DDD simulations, a theoretical model is constructed to further understand the physical and distinct origins of deformation localization. A cross slip induced dislocation channel widening model is first developed as depicted in Fig. 4(a). Assuming that characteristic double cross slip height is h_{cs}, and dislocations have a probability q of double cross slip after gliding a distance L_{cs}, with equal probability $q/2$ of reaching upper and lower slip planes. Similar to a branching process described in Fig. 4(a), after gliding a distance nL_{cs}, the probability $P(n, j, q)$ of reaching a slip plane with distance jh_{cs} away from the original slip plane is,

TABLE I. Theoretical model parameters.

α_1	α_2	k_m	y_a	λy	h_{cs}
0.35 [38]	0.3 [21]	0.01 [39]	0.6b [40]	8.4b [21]	10b [40]

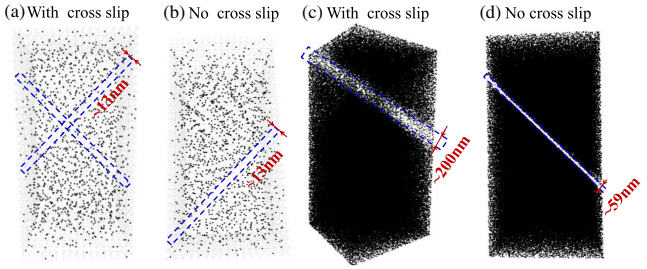

FIG. 3. Results of 3D-DDD simulations of dislocation channel formation in high-dose irradiated pillars when the plastic strain is 2.0%. For (a)–(b) $d = 300$ nm, and (c)–(d) $d = 1500$ nm. The width of the channel is indicated. Note that cross slip is not essential for channel formation.

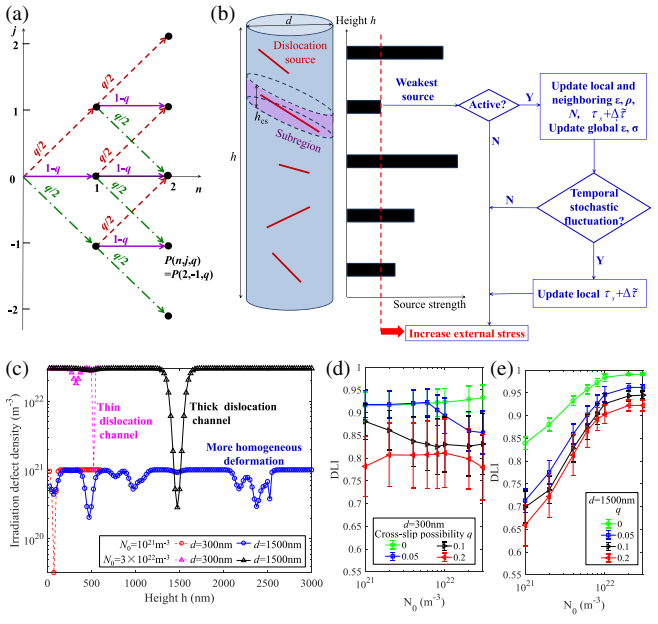

FIG. 4. Schematic illustrating (a) cross slip induced channel widening model and (b) the discrete dislocation source activation model. (c)–(e) The predicted results when the plastic strain is 2.0%. The DLI is the average over 1000 realizations.

$$P(n,j,q) = \sum_{n_-=\max(-j,0)}^{n_-\le(n-j)/2} \frac{n!}{(j+n_-)!(n-j-2n_-)!n_-!} \times \left(\frac{q}{2}\right)^{j+n_-} (1-q)^{n-j-2n_-} \left(\frac{q}{2}\right)^{n_-}, \quad (6)$$

where n_- is non-negative integer describing the number of downward cross slip events [22]. $-n \le j \le n$. j reflects the channel widening magnitude, while n captures the size truncation effect since $n = d/L_{cs}$. $P(n,j,q)$ is a cumulative trinomial distribution, representing the channel widening probability if n keeps constant during deformation. Suppose that each time dislocations meet the irradiation defect, one cross slip event may occur. Accordingly, L_{cs} is set to $N^{(1/3)}$, where N is local irradiation defect density. Therefore, during the deformation, n varies with N.

In the following, a simple 2D Monte Carlo model is developed by coupling the DDD-informed dislocation source activation mechanism and the cross slip induced channel widening model. First, the sample is divided into multiple subregions by cross slip height h_{cs} along the sample height h, as schematically shown in Fig. 4(b). Dislocation sources are assumed to be distributed uniformly, with a total number $\rho V/\bar{L}$ [39]. Here, V is the sample volume and $\bar{L}$ is the average effective source length. This naturally reproduces the feature of limited dislocation sources at small scales [42]. The source strength is $\tau_s + \Delta\tilde{\tau}$, where τ_s is evaluated by Eq. (1). $\Delta\tilde{\tau}$ depends on the effective local source length, source type, slip system, etc. For simplicity, all of these factors are lumped into the variations of the effective source length [43]. Similar to 2D-DDD simulations [44], the source length L follows a Gaussian distribution, with a mean value $\bar{L}$, and standard deviation $20\%\bar{L}$ [45]. At small scales, $\Delta\tilde{\tau} = \alpha_3\mu b/L$ [45], where α_3 is a dimensionless constant. $\bar{L}$ is $0.317d$ to model the truncation effect induced by the external size [39]. For a bulklike sample, the spatial heterogeneity of source strength is mainly induced by the character and the arrangement of dislocations. Therefore, $\Delta\tilde{\tau}$ is assumed to fluctuate around the Taylor resistance stress. Namely, $\Delta\tilde{\tau} = \alpha_1\mu b/L - \alpha_1\mu b/\bar{L}$. $\bar{L}$ is $1/\sqrt{\rho}$ [37].

As depicted by the flowchart in Fig. 4(b), the weakest source (with the lowest strength) activates first during deformation. When the dislocation source sweeps the whole slip system once, the plastic strain increases by $b\cos\beta/h_{cs}$ [45], where β is the angle between the slip-plane normal of this source and the loading axis. To consider the spatial coupling arising out of the double cross slip mechanism, this plastic strain is assumed to spread to the neighboring $2n$ subregions by multiplying with the widening probability in Eq. (6). Then, the neighboring and local irradiation defect density and dislocation density evolve by Eqs. (2) and (3), respectively. In order to consider the temporal fluctuation of local coarse-grained resistance stress, induced by complex dislocation-dislocation and dislocation-defect interactions, a random number k is generated between 0 and 1. If $k < P_{tf}$, the local dislocation source strength fluctuates by randomly resetting a new source length. If the new source is much stronger, it means the local source is exhausted, or it is strongly pinned. This process is repeated until the end of the desired deformation.

Typical prediction results obtained by this simple model, using parameters listed in Table I, are demonstrated in Figs. 4(c)–(e). In bulklike samples, a significant dose-dependent irradiation defect distribution and DLI are observed in Figs. 4(c) and 4(e) after deformation. By contrast, the DLI at small scales shows a weaker dose sensitivity. In Fig. 4(d), the tendency of the weak inverse dose dependence is a result of the interaction with irradiation defects, which promote dislocation cross slip. Such a trend is difficult to observe at a small size (300 nm) due to the significant scatter. In addition, the size-dependent dislocation channel widths are captured in Fig. 4(c). This model can also capture the yield drop feature in the stress-strain curve (see Fig. S6 in Supplemental Material [22]) that is observed experimentally. The excellent agreement between these abstract 2D model predictions and the more fundamental 3D-DDD simulations and experimental observations [35] verifies the basic physics of the simple model, and it shows that it may be used to guide the design of new irradiation-resistant materials. For example, cross slip probability q can be tuned by changing the stacking fault energy and temperature etc. Figures 4(d)–(e) show that

tuning q does not qualitatively affect the dose sensitivity of the DLI, but increasing cross slip probability decreases the DLI by increasing the channel width. Here, P_{tf} is 0.2. A sensitivity analysis of the choice of P_{tf} from 0.05 to 0.2 shows a small decrease in the DLI (see Fig. S5). This implies that the source strength fluctuation induced by local entrapment or dislocation interactions promotes a more homogeneous deformation.

In conclusion, an easy-to-handle parameter deformation localization index is proposed to quantitatively assess the localization extent of plastic deformation. We demonstrate that at small scales, the plastic flow localization mode transitions from irradiation-defect clearing controlled to an intrinsic limited dislocation source dominated mechanism. The dislocation channel width at the same plastic strain is shown to be reduced when cross slip is not very active, indicating that cross slip is not necessary to the creation of the channel, but it is beneficial since it spreads plastic strain over larger volumes. Based on the insights gained from the DDD simulations, a simple model based on cross slip channel widening coupled with stochastic glide is developed. The model reproduces the size effects on deformation localization. This study also sheds light on understanding the deformation localization issue in barrier-strengthened materials (e.g., nanoprecipitates), and it has implications in the design of new radiation-resistant materials by tuning size and other microstructural parameters, such as stacking fault energy and dislocation density.

This material is based upon work supported by the U.S. Department of Energy, Office of Science, Office of Fusion Energy Sciences, under Award No. DE-SC0018410. We would like to thank Prof. Jaime Marian (UCLA, USA) and Prof. Laurent Ponson (Université Pierre et Marie Curie, France) for inspiring comments and discussions.

*cuiyinan@ucla.edu

[1] A. Le Bouil, A. Amon, S. McNamara, and J. Crassous, Phys. Rev. Lett. **112**, 246001 (2014).
[2] C. Healy, S. Koch, C. Siemers, D. Mukherji, and G. J. Ackland, Phys. Rev. Lett. **114**, 165501 (2015).
[3] D. Marsan, H. Stern, R. Lindsay, and J. Weiss, Phys. Rev. Lett. **93**, 178501 (2004).
[4] T. D. de la Rubia, H. M. Zbib, T. A. Khraishi, B. D. Wirth, M. Victoria, and M. J. Caturla, Nature (London) **406**, 871 (2000).
[5] H. Bei, S. Xie, and E. P. George, Phys. Rev. Lett. **96**, 105503 (2006).
[6] P. Sedmák, J. Pilch, L. Heller, J. Kopeček, J. Wright, P. Sedlák, M. Frost, and P. Šittner, Science **353**, 559 (2016).
[7] D. Rodney and G. Martin, Phys. Rev. Lett. **82**, 3272 (1999).
[8] Y. Fan, Y. N. Osetskiy, S. Yip, and B. Yildiz, Proc. Natl. Acad. Sci. U.S.A. **110**, 17756 (2013).
[9] M. S. Ding, L. Tian, W. Z. Han, J. Li, E. Ma, and Z. W. Shan, Phys. Rev. Lett. **117**, 215501 (2016).
[10] N. Ghoniem, S.-H. Tong, B. Singh, and L. Sun, Philos. Mag. A **81**, 2743 (2001).
[11] J. Robach, I. Robertson, B. Wirth, and A. Arsenlis, Philos. Mag. **83**, 955 (2003).
[12] A. Arsenlis, M. Rhee, G. Hommes, R. Cook, and J. Marian, Acta Mater. **60**, 3748 (2012).
[13] D. Kiener, P. Hosemann, S. Maloy, and A. Minor, Nat. Mater. **10**, 608 (2011).
[14] P. Hosemann, Scr. Mater. **143**, 161 (2018).
[15] E. Grieveson, D. Armstrong, S. Xu, and S. Roberts, J. Nucl. Mater. **430**, 119 (2012).
[16] X. Zhao, D. J. Strickland, P. M. Derlet, M.-r. He, Y.-J. Cheng, J. Pu, K. Hattar, and D. S. Gianola, Acta Mater. **88**, 121 (2015).
[17] G. Po and N. Ghoniem, https://bitbucket.org/model/model/wiki/Home.
[18] G. Po and N. Ghoniem, J. Mech. Phys. Solids **66**, 103 (2014).
[19] G. Po, Y. Cui, D. Rivera, D. Cereceda, T. D. Swinburne, J. Marian, and N. Ghoniem, Acta Mater. **119**, 123 (2016).
[20] Y. Cui, G. Po, and N. Ghoniem, Acta Mater. **132**, 285 (2017).
[21] Y. Cui, G. Po, and N. Ghoniem, Int. J. Plast. **104**, 54 (2018).
[22] See Supplemental Material at http://link.aps.org/supplemental/10.1103/PhysRevLett.120.215501 for more discussions about simulation methods and theoretical models, which includes Refs. [23–34].
[23] N. Ghoniem, B. Singh, L. Sun, and T. D. de la Rubia, J. Nucl. Mater. **276**, 166 (2000).
[24] D. Rodney, G. Martin, and Y. Bréchet, Mater. Sci. Eng. A **309**, 198 (2001).
[25] Y. N. Osetsky, R. E. Stoller, D. Rodney, and D. J. Bacon, Mater. Sci. Eng. A **400**, 370 (2005).
[26] S. J. Zinkle and B. N. Singh, J. Nucl. Mater. **351**, 269 (2006).
[27] D. Bacon, Y. Osetsky, and D. Rodney, Dislocat. Solids **15**, 1 (2009).
[28] Y. N. Osetsky and D. J. Bacon, Philos. Mag. **90**, 945 (2010).
[29] G. Monnet, Y. N. Osetsky, and D. J. Bacon, Philos. Mag. **90**, 1001 (2010).
[30] G. Bonny, D. Terentyev, J. Elena, A. Zinovev, B. Minov, and E E. Zhurkin, J. Nucl. Mater. **473**, 283 (2016).
[31] Y. Chen, P. Spätig, and M. Victoria, J. Nucl. Mater. **271**, 128 (1999).
[32] D. Terentyev, G. Monnet, and P. Grigorev, Scr. Mater. **69**, 578 (2013).
[33] M. D. Uchic, P. A. Shade, and D. M. Dimiduk, Annu. Rev. Mater. Res. **39**, 361 (2009).
[34] J. Sharp, Radiat. Eff. **14**, 71 (1972).
[35] B. Singh, A. Horsewell, and P. Toft, J. Nucl. Mater. **271**, 97 (1999).
[36] A. Patra and D. L. McDowell, Acta Mater. **110**, 364 (2016).
[37] B. Devincre, T. Hoc, and L. Kubin, Science **320**, 1745 (2008).
[38] H. Mughrabi, Curr. Opin. Solid State Mater. Sci. **20**, 411 (2016).
[39] Y. Cui, P. Lin, Z. Liu, and Z. Zhuang, Int. J. Plast. **55**, 279 (2014).

[40] L. P. Kubin, G. Canova, M. Condat, B. Devincre, V. Pontikis, and Y. Bréchet *et al.*, Solid State Phenom. **23**, 455 (1992).
[41] D. Dimiduk, M. Uchic, and T. Parthasarathy, Acta Mater. **53**, 4065 (2005).
[42] A. Ngan, X. Chen, P. Leung, R. Gu, and K. Gan, MRS Commun. **7**, 131 (2017).
[43] S.-W. Lee and W. D. Nix, Philos. Mag. **92**, 1238 (2012).
[44] S. Papanikolaou, H. Song, and E. Van der Giessen, J. Mech. Phys. Solids **102**, 17 (2017).
[45] Y. Cui, G. Po, and N. Ghoniem, Phys. Rev. Lett. **117**, 155502 (2016).